The Atlantic Subtropical Cells Inferred from Observations

Franz Philip Tuchen[1] [ID], **Joke F. Lübbecke[1,2]** [ID], **Sunke Schmidtko[1]** [ID], **Rebecca Hummels[1]**, and **Claus W. Böning[1,2]** [ID]

[1]GEOMAR Helmholtz Centre for Ocean Research Kiel, Kiel, Germany, [2]Faculty of Mathematics and Natural Sciences, Kiel University, Kiel, Germany

Abstract The Atlantic Subtropical Cells (STCs) are shallow wind-driven overturning circulations connecting the tropical upwelling areas to the subtropical subduction regions. In both hemispheres, they are characterized by equatorward transport at thermocline level, upwelling at the equator, and poleward Ekman transport in the surface layer. This study uses recent data from Argo floats complemented by ship sections at the western boundary as well as reanalysis products to estimate the meridional water mass transports and to investigate the vertical and horizontal structure of the STCs from an observational perspective. The seasonally varying depth of meridional velocity reversal is used as the interface between the surface poleward flow and the thermocline equatorward flow. The latter is bounded by the $26.0 \, \text{kg m}^{-3}$ isopycnal at depth. We find that the thermocline layer convergence is dominated by the southern hemisphere water mass transport (9.0 ± 1.1 Sv from the southern hemisphere compared to 2.9 ± 1.3 Sv from the northern hemisphere) and that this transport is mostly confined to the western boundary. Compared to the asymmetric convergence at thermocline level, the wind-driven Ekman divergence in the surface layer is more symmetric, being 20.4 ± 3.1 Sv between 10°N and 10°S. The net poleward transports (Ekman minus geostrophy) in the surface layer concur with values derived from reanalysis data (5.5 ± 0.8 Sv at 10°S and 6.4 ± 1.4 Sv at 10°N). A diapycnal transport of about 3 Sv across the $26.0 \, \text{kg m}^{-3}$ isopycnal is required in order to maintain the mass balance of the STC circulation.

Plain Language Summary The Atlantic Subtropical Cells (STCs) are shallow wind-driven overturning circulations connecting the tropics to the subtropical regions within the upper 300 m. In both hemispheres, they are characterized by equatorward transport at subsurface level and poleward transport in the surface layers. They are closed by upwelling at the equator and subduction in the subtropics. STCs are suggested to impact sea-surface temperature variability in tropical upwelling regions thereby influencing, for example, precipitation patterns. The boundary between the two branches is approximated by the depth at which the meridional velocity reverses. The lower boundary of the deep equatorward branch is defined by an isoline of potential density. We find that at subsurface level, the equatorward branches converge in the tropics with more transport coming from the southern hemisphere. At the surface, a more symmetric divergence of water mass is observed in the tropics. The surface layers are also influenced by geostrophic transport generally counteracting the wind-driven divergence. In total, the net surface divergence and the subsurface convergence yield a residual. It is suggested that this water mass volume deficit originates from below the STCs and enters the subsurface layers in the tropics where it is lifted to the surface.

1. Introduction

The subduction zones in the oceanic subtropical gyres are linked to the tropics by shallow meridional overturning circulations confined to the upper approximately 300 m: the Subtropical Cells (STCs). The STCs are driven by poleward Ekman transport within the surface layer in the tropics, forming the equatorial divergence. In the subtropics, Ekman pumping causes subduction of water masses to thermocline level. From here, geostrophic transport brings the water back toward the equator along isopycnal surfaces. In the tropics, equatorial upwelling due to Ekman divergence or coastal upwelling forms the last branch of the STCs (e.g., Liu et al., 1994; McCreary & Lu, 1994; Schott et al., 2004).

The STCs upwell cool subsurface waters and thereby maintain the tropical thermocline (Schott et al., 2004). Variations in the mean water mass transports due to STC dynamics enable advection of hydrographic and/or

transport anomalies from the subtropics to the equator. Hence, STCs are suggested to influence equatorial sea-surface temperature (SST) variability on interannual to decadal time scales in the tropical Atlantic Ocean via two different processes (Schott et al., 2004). In the first process, temperature anomalies are subducted in the subtropics and transported at the thermocline level toward the equatorial or eastern tropical upwelling regions impacting tropical SST (Gu & Philander, 1997). The second process describes an anomalous equatorward thermocline transport that changes the amount of thermocline water entering the upwelling regions rather than its properties (Kleeman et al., 1999). For the Pacific Ocean, the second process has been shown to play an active role in both models and observations, resulting in pronounced SST anomalies in the eastern equatorial upwelling area (Farneti et al., 2014; Lübbecke et al., 2008; McPhaden & Zhang, 2002, 2004).

Despite the simplified model of overturning described above, STCs are far from being two-dimensional and exhibit rather complex pathways. Subduction in the subtropical Atlantic generally occurs in the eastern parts of the basins driven mainly by Ekman pumping. From there, subducted water flows westward and equatorward (e.g., Lazar et al., 2002) while zonal currents distort their pathways. Malanotte-Rizzoli et al. (2000) showed that for subducted water masses, three different pathways exist between the subtropics and tropics. First, thermocline water can reach the equatorial upwelling zones on interior routes. Second, depending on the latitude of subduction, thermocline water can reach the western boundary where it is entrained in the western boundary current and travels equatorward. Third, thermocline water that reaches the western boundary too far south in the southern hemisphere or too far north in the northern hemisphere is recirculated poleward within the subtropical gyre and does not participate in the subtropical-tropical exchange. These theoretical pathways are modified in the northern hemisphere by the presence of the Intertropical Convergence Zone (ITCZ) between $5° - 15°$N. Upwelled waters within the ITCZ have a higher PV and are more stratified than subducted waters at the same density range. Thermocline water is forced to circumvent the PV barrier which extends roughly from 15°N in the central eastern part of the basin to 10°N near the western boundary (Harper, 2000) causing thermocline water on equatorward pathways to take a westward detour (Zhang et al., 2003) largely hindering interior pathways in the northern hemisphere.

The interhemispheric asymmetry is increased by the return flow of the Atlantic Meridional Overturning Circulation (AMOC) superimposed upon the Atlantic STCs which is particularly apparent at the western boundary (e.g., Fratantoni et al., 2000; Hazeleger & Drijfhout, 2006). In the southern tropical Atlantic, the upper ocean return flow of the AMOC is focused in the northward flowing North Brazil Undercurrent (NBUC) which loses its undercurrent character on its equatorward pathway after being augmented by the shallower inflow of the South Equatorial Current (Schott et al., 2004). It then continues as the surface-intensified North Brazil Current (NBC) crossing the equator and transporting warm water northward. Hence, the upper ocean return flow of the AMOC strengthens the southern hemisphere STC while countering southward thermocline transports in the northern hemisphere STC (e.g., Schott et al., 2004) along the western boundary. As a consequence, the Equatorial Undercurrent (EUC) is predominantly fed by thermocline water of South Atlantic origin (Fratantoni et al., 2000; Harper, 2000; Hazeleger et al., 2003; Liu et al., 1994; Tsuchiya, 1986) leading to an asymmetry of origins of water masses within the density range of the equatorward branch (Peña-Izquierdo et al., 2015; Oschlies et al., 2018). Therefore, central and intermediate waters in the tropical North Atlantic are mainly ventilated by waters originating in the South Atlantic. Analogously, the Indonesian throughflow is responsible for a similar asymmetry of the STCs in the Pacific Ocean. There, an estimated 80–90% of EUC water originates in the southern hemisphere (Kuntz & Schrag, 2018; Schott et al., 2004) which is comparable to Atlantic Ocean estimates by Fratantoni et al. (2000) that 85% of the water masses transported by the EUC in the western Atlantic originate in the South Atlantic.

Most of the STC characteristics described so far have been derived from model studies. Observational estimates of transport values for the individual branches of the Atlantic STCs (thermocline layer transport and surface layer transport in both hemispheres) have been provided by Zhang et al. (2003) based on five decades of hydrographic data mainly from the World Ocean Database and the World Ocean Circulation Experiment. Their calculations showed that on average, 5 Sv ($= 10^6$ m^3s^{-1}) northern hemisphere waters (2 Sv interior and 3 Sv western boundary) and 10 Sv southern hemisphere waters (4 Sv interior and 6 Sv western boundary) reach the equator. Aside from Zhang et al. (2003), observational efforts studying the Atlantic STCs have been rare. However, numerical model studies such as Hazeleger and Drijfhout (2006) estimate STC transports from a high-resolution model to be more than a factor of 2 smaller than the observational estimates (4 Sv from the south and 1.5 Sv from the north). Moreover, Fratantoni et al. (2000) use an eddy-resolving ocean circulation model to design different model experiments with and without a meridional overturning
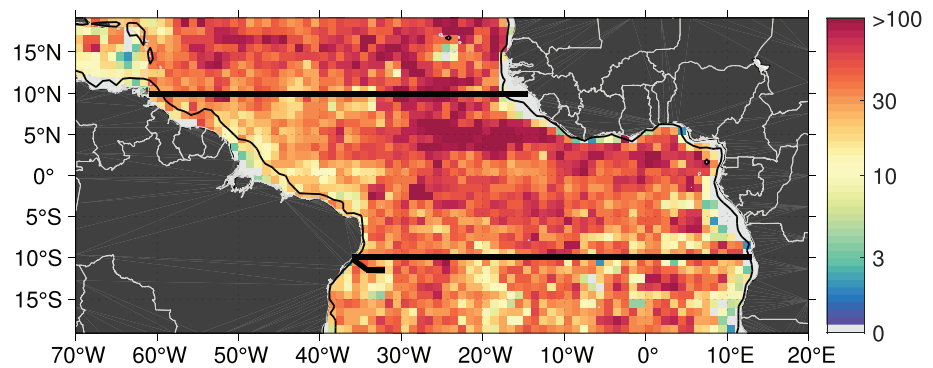
Figure 1. Number of Argo profiles (delayed mode) within horizontal boxes of $(1°)^2$ between 2004 and 2016. Note the logarithmic color scale. Zonal sections at 10°N, 10°S and a repeated ship section at the western boundary are marked (thick black lines). The 1,000-m isobath from the ETOPO1 bathymetry (Amante & Eakins, 2009) is superimposed (black contours).

circulation. Their results show that the combination of wind and MOC forcing yields an asymmetric thermocline convergence of 14 Sv southern hemisphere and 2 Sv northern hemisphere contribution while their wind-only experiment shows a symmetric thermocline convergence among hemispheres of 8 Sv from the southern hemisphere and 7 Sv from the northern hemisphere. However, the asymmetry between interior transport and western boundary transport remains. In addition, the transports of the solutions of the wind + MOC forced run are a superposition of the transports of the wind-only and MOC-only runs. The linearity does not hold for the mesoscale variability which is greatly enhanced in the MOC including runs. Other studies further emphasize how the choice of wind stress forcing influences the overall circulation patterns and the exchange windows in general circulation models. For instance, Inui et al. (2002) and Lazar et al. (2002) both show that a stronger wind stress forcing causes the interior exchange windows to be of smaller extent. However, the discrepancy in STC transports between model studies and Zhang et al. (2003) emphasizes the need of further studies based on observations.

When estimating their transport, STCs have to be distinguished from the tropical cells (TCs) which are shallow tropical overturning circulations close to equator. The latitudinal extent of the TCs is approximately ±3.5° off the equator (e.g., Lu et al., 1998) suggesting that the TCs mainly recirculate tropical water masses and do not participate in the subtropical-tropical water mass exchange. However, at equatorial latitudes, they superimpose upon the STCs and therefore zonal sections of thermocline equatorward transport associated with the STCs should be calculated poleward of the TCs. The present study focuses on the Atlantic STCs, and in the following, any use of the abbreviation STC will refer to the cells of the Atlantic Ocean, unless otherwise noted. Observations in the Atlantic Ocean have multiplied—especially due to the Argo program—since the transport estimates of Zhang et al. (2003). Furthermore, the enhanced spatial and temporal coverage of the last two decades calls for an updated observational estimate of the STC transports to allow for a more detailed investigation of their structure.

This study is structured as follows. First, the different data sets are described in section 2. Section 3 provides a summary of the methods used to calculate the individual STC branches and their error estimate. Section 4 describes the results which are divided into thermocline transports and surface transports. In section 5 the presented results are summarized and discussed.

2. Data

2.1. Argo Climatological Data

Since its start in 2000, the Argo program has grown into a global array of nearly 4,000 profiling floats. This coverage has been sustained for more than a decade, providing temperature and salinity profiles in the upper 2,000 m (Figure 1). Overall, more than 160,000 Argo profiles are available between 20°S and 20°N in the Atlantic for the time period of 2004 to 2016. This is approximately the same number of hydrographic profiles that Zhang et al. (2003) used for a period spanning five decades, though their latitudinal range (40°S to 50°N) is more than twice the range analyzed here (see their Figure 1), indicating a data density half of what is available for this study.

Within the framework of this study, monthly geostrophic transports are calculated from the 2017 version of the Roemmich-Gilson Argo climatology (from here on called RG-clim; Roemmich & Gilson, 2009). The updated version of the RG-clim is based on a similar analysis method as in Roemmich and Gilson (2009) and available for the time period from 2004 to 2016 providing (a) a climatological mean and (b) monthly anomalies of temperature and salinity both mapped on a 1° x 1°grid and on 58 depth levels. For a detailed description of how the RG-clim is derived, the mapping methods and the additional quality control criteria applied to the available Argo profiles, see Roemmich and Gilson (2009).

2.2. Western Boundary Ship Section

The western boundary is generally a region of sparse Argo float coverage (Figure 1). However, it is a key region for equatorward STC transports. In order to better resolve the southern hemisphere western boundary, five individual sections of hydrographic and acoustic Doppler current profiler (ADCP) measurements are used to construct mean sections of conservative temperature, absolute salinity, and alongshore/meridional velocity. All cruises were carried out with the RV Meteor in July 2013 (M98), May 2014 (M106), October 2015 (M119), September 2016 (M130), and March 2018 (M145). Shipboard ADCP data are combined with lowered ADCP profiles at hydrographic stations to construct full-depth velocity sections (e.g., Hummels et al., 2015).

The mean section is an update of Hummels et al. (2015) but only implements sections from 2013 onward. All cruise tracks followed 11.5°S between 32°W and 34.15°W before turning northwestward toward the Brazilian coast where the sections end at 36°W and 10.2°S (Figure 1). Alongshore velocity from the cross-shore ship section is combined with meridional velocities from the zonal part of the ship section.

Shipboard velocity measurements used in this study are in good agreement with the mean alongshore velocity section derived from moored observations along 11.5°S (e.g., Hummels et al., 2015). Variability on seasonal time scales has been estimated by Schott et al. (2005) for an earlier period of the mooring array. They found a seasonal cycle of NBUC transport with a range of about 4 Sv between a maximum in July and a minimum in October/November which is most likely covered by the somewhat evenly distributed sections (March, May, July, September, and October). This encouraged us to use the spatially high-resolved mean ship section for further analysis.

2.3. Monthly Isopycnal and Mixed-layer Ocean Climatology

The Monthly Isopycnal and Mixed-layer Ocean Climatology (MIMOC; Schmidtko et al., 2013) provides hydrographic climatological monthly means based on Argo profiles, shipboard, and ice-tethered CTD data and profiles archived in the World Ocean Database. Climatological profiles are mapped with a horizontal resolution of $(0.5°)^2$ and on 81 pressure levels between 0 and 1,950 dbar. MIMOC is intended to represent the modern state of the world oceans meaning that recent observations are emphasized. However, in regions with poor data coverage, the climatology relaxes to historic data from as early as the 1970s. Due to the incorporation of CTD data, MIMOC can provide useful insights inshore of the 1,000-m isobath where Argo profiles are absent.

2.4. Ocean Reanalysis 4

Thermocline transport estimates are evaluated by comparison of observational data with the ECMWF Ocean Reanalysis 4 (ORA-S4; Balmaseda et al., 2013). ORA-S4 has a horizontal resolution of $(1°)^2$ and covers a time period between 1958 and 2017 of which we use hydrographic and velocity data between 2000 and 2017. In addition to potential temperature and practical salinity profiles which are converted into conservative temperature and absolute salinity profiles and from which geostrophic transports are calculated, ORA-S4 further provides zonal and meridional velocity data on 42 depth levels. Absolute velocity data are used here for comparison and to determine the depth at which the meridional velocity reverses from poleward at the surface to equatorward at thermocline depth. This depth is taken to represent the interface between the upper and the lower STC branches as described in section 3.2.

2.5. Wind Products

Surface transports of the STCs are associated with poleward Ekman transport. In order to estimate the meridional Ekman transport, wind stress data from several products are used. The Advanced Scatterometer (ASCAT) satellite observations provide daily maps of surface wind speed with a horizontal resolution of 25 km for the time period between 2007 and 2018. Satellite observations from ASCAT are complemented by the NCEP/NCAR Reanalysis I which provides 6-hourly wind speed data on a $(2.5°)^2$ horizontal grid and by

JRA-55 6-hourly wind speed data on a $(0.5°)^2$ grid from which the zonal surface wind stress (τ_x) is calculated via the Bulk formula:

$$\tau_y = \rho_a * c_d * u^2 \tag{1}$$

using a reference density $\rho_a = 1.22$ kg m^{-3}, a drag coefficient $c_D = 0.0013$ (used, e.g., in Kopte et al., 2018) and the zonal surface wind speed u.

3. Methods
3.1. Thermocline Transport
In a first step, the gridded hydrographic data (available either as in situ temperature or potential temperature and practical salinity) are converted into conservative temperature (CT) and absolute salinity (S_A) following the definitions of the TEOS-10 (McDougall, 2017). From CT and S_A, profiles of dynamic height are calculated at each longitude of the zonal sections at 10°N and 10°S. These latitudes are chosen because of their sufficient distance from the TCs close to the equator on the one side and to the subtropical subduction zones on the other side. In addition, we can combine estimates at 10°S with the close-by repeated ship section at 11.5°S. All thermocline water associated with the STCs has to pass these latitudes on either interior or western boundary pathways. Zonal sections of dynamic height are used to derive zonal pressure gradients (p_x) from which relative meridional geostrophic velocities (v_g) perpendicular to the zonal sections are calculated:

$$-f(y)\, v_g = -\frac{1}{\rho_0}\, p_x, \tag{2}$$

where f represents the Coriolis parameter at the specific latitude (y) of the section and ρ_0 a reference density. Absolute geostrophic velocities are inferred with a reference level based on the time-mean meridional displacement of Argo floats at their parking level derived from the YoMaHa'07 data set (Lebedev et al., 2007). The majority of the Argo floats drift at a deep parking level of around 1,000 dbar. Consequently, absolute geostrophic velocities derived from the RG-clim and MIMOC are referenced to this level of known motion. Note that absolute velocities at 1,000 dbar from ORA-S4 are indistinguishable from zero. Therefore, geostrophic velocities from ORA-S4 are inferred with an assumed reference level of no motion at 1,000 dbar.

CT and S_A are used to calculate mean sections of potential density along 10°N and 10°S. Equatorward transports from geostrophic and absolute velocities are calculated between an upper boundary and a lower boundary which is discussed in detail below in section 4.1. The layer thickness (Δz) between these boundaries at each longitude, latitude, and time step, the zonal grid space (Δx), and the monthly meridional (geostrophic or total) velocity (v) within the layer are needed to calculate the monthly meridional (geostrophic or total) volume transport (T) at each longitude (x), latitude (y), and time step (t):

$$T(x, y, t) = \Delta x\, \Delta z(x, y, t)\, v(x, y, t). \tag{3}$$

The estimate of transport uncertainties in thermocline layer and surface layer transport (shown in Tables 1 and 2) is given by the temporal standard deviation at each longitude along the zonal sections at 10°N and 10°S. While the transport is accumulated along zonal sections by summing from east to west, the uncertainties of the cumulative transport estimates (ϵ) are calculated by using the rules of error propagation:

$$\epsilon = \sqrt{\sum_i \sigma_i^2}, \tag{4}$$

where σ_i is the temporal standard deviation at longitude i.

3.2. Surface Transport
The poleward surface transport of the STCs is calculated using wind stress data derived from several wind products (see section 2.5): ASCAT, JRA-55, and NCEP/NCAR Reanalysis I. Under the assumption that the poleward surface transport associated with the upper branch of the STCs is driven by the meridional Ekman transport, the surface transport (T_E) is defined by

$$T_E(x, y, t) = -\frac{1}{\rho_0}\, \frac{\tau_x(x, y, t)}{f(y)}\, \Delta x, \tag{5}$$

where τ_x represents the zonal wind stress for a given horizontal cell (Δx). Surface transports are calculated for each time step (t) before averaging over time.
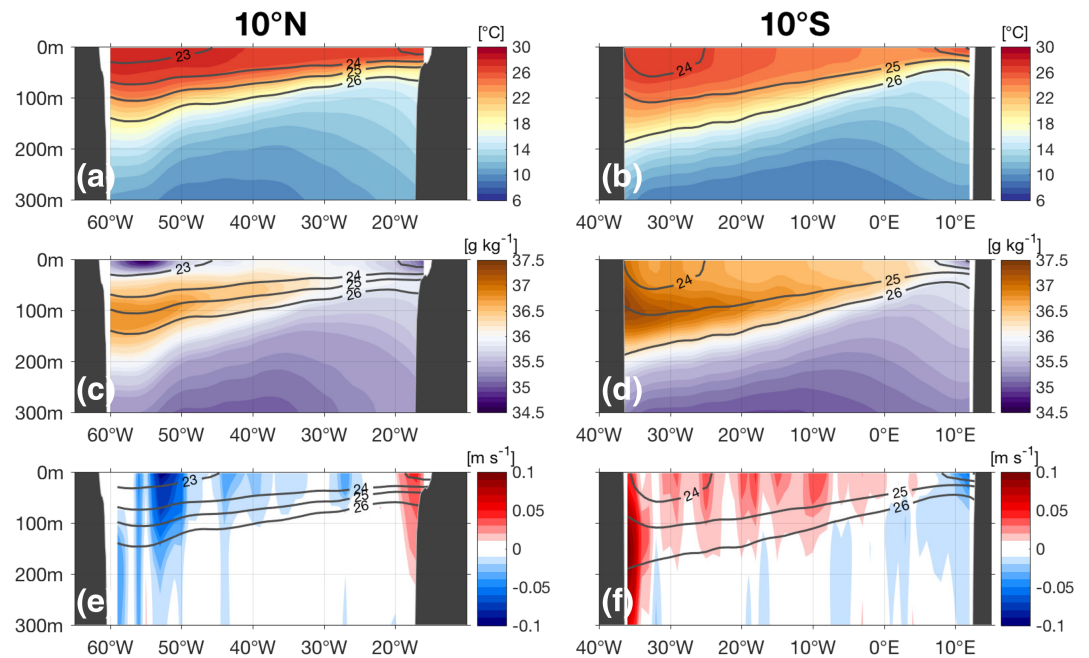
Figure 2. Zonal sections of (a)–(b) conservative temperature, (c)–(d) absolute salinity, and (e)–(f) meridional geostrophic velocity along 10°N (left column) and 10°S (right column) from the RG-clim mean (see section 2.1 for detailed description). Isopycnal surfaces are shown as black contour lines. A realistic topography from the ETOPO1 data set shows the eastern and western boundaries of the sections.

4. Results

4.1. Thermocline Transports

The STCs are divided into a subsurface equatorward and a surface poleward branch. In the following, the transports of the equatorward branches are estimated individually along two zonal sections at 10°N and 10°S. Hydrographic properties, CT and S_A, along these sections are presented from the RG-clim (Figures 2a to 2d). They show the tilted thermocline/halocline/pycnocline toward the east of the basin, which is steeper in the southern hemisphere, as well as a fresh water lens at 10°N (Figure 2c) close to the western boundary that is most likely associated with the Amazon and Orinoco river outflow a few degrees to the south. In the central and eastern part of the northern section, the mean position of the ITCZ leads to decreased sea surface salinity and a subsurface salinity maximum. The southern section generally exhibits higher salinity in the surface layer and shows a subsurface maximum close to the western boundary.

Zonal sections of CT and S_A are used to calculate meridional geostrophic velocity across 10°N and 10°S (Figures 2e to 2f). Between the surface and approximately the 26.0 kg m^{-3} isopycnal, the meridional geostrophic flow is mainly equatorward except for at the eastern boundary where both sections reveal poleward flow. At 10°S, the western boundary shows the geostrophic part of the equatorward flowing NBUC with maximum geostrophic velocities of about 0.2 m s^{-1}. This is about half the magnitude of absolute velocities measured by Hummels et al. (2015). Since western boundary currents are mainly in geostrophic balance, this difference likely indicates an underestimation of the NBUC by the RG-clim. On its equatorward path, the NBUC is augmented by the shallower inflow of the low-latitude South Equatorial Current and continues northward as the surface intensified NBC (e.g., Schott et al., 1998). The NBC is poorly sampled at the northern section due to sparse data coverage (Figure 1). Potential consequences of the deficient representation of the NBC for the transport estimates of the STCs are discussed below in section 5. Nevertheless, the southward recirculation of the NBC between 50 and 55°W at 10°N is well captured.

In order to calculate equatorward volume transports associated with the STCs, first, the vertical extent of the layer in which the lower branches of the STCs reside has to be defined. This layer is called the thermocline layer. First, we focus on the lower boundary.

In general, the vertical structure of meridional geostrophic transports per 0.2 kg m^{-3} density bin agrees well for the different geostrophic products (Figure 3). At 10°N, the deepest layers below 26.0 kg m^{-3} show
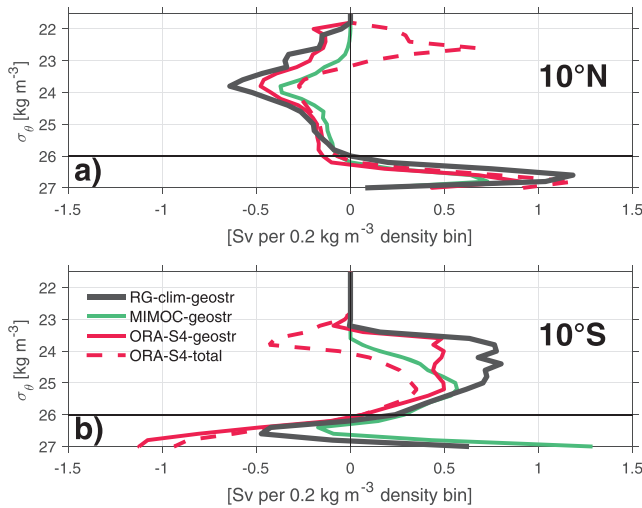
Figure 3. Averaged meridional transport per 0.2 kg m^{-3} density bin for (a) 10°N and (b) 10°S from the African coast to (a) 55°W and (b) 32°W thereby excluding the western boundary. Values show the transport within ±0.1 kg m^{-3} of the isopycnal on the y-axis.

poleward transport in all products, with a peak at about 26.5 kg m^{-3} in the RG-clim and slightly deeper in ORA-S4 and MIMOC indicating the interior northward pathway of the thermohaline circulation (Figure 3a). Generally, the sign of transport changes from poleward to equatorward right above 26.0 kg m^{-3}. Hence, the 26.0 kg m^{-3} isopycnal is chosen as the lower boundary of the northern STC. Total meridional transport derived from absolute velocity data from ORA-S4 includes the poleward Ekman transport in the surface layer and therefore differs from the geostrophic transports above a certain isopycnal surface which can be seen as a proxy for the zonal mean potential density equivalent of the annual mean Ekman depth. At 10°S, the vertical structure of meridional transport is basically mirroring the structure of the northern section (Figure 3b). Below 26.0 kg m^{-3}, poleward transport represents the recirculation of the South Equatorial Undercurrent (Stramma & Schott, 1999). Northward transport below 26.5 kg m^{-3} as seen in RG-clim and MIMOC indicates the northward flow of Antarctic Intermediate Water which is not seen in ORA-S4 transports. Closer to the surface and above 26.0 kg m^{-3}, equatorward transport is observed with peak values between 23.5 and 25 kg m^{-3}. Analogously to the northern section, we choose the 26.0 kg m^{-3} isopycnal as the lower boundary of the equatorward branch of the STC at 10°S.

In Figure 3, we observe a change of sign in ORA-S4 data at lighter water masses and therefore closer to the surface, which could be indicative for the upper boundary of the lower STC branches. However, Figure 2 shows that choosing an isopycnal for the lower boundary is justified as the sign of flow follows isopycnal surfaces while in the surface layers, isopycnal surfaces could intersect the Ekman layer in the east and the flow is not only a function of potential density anymore. The choice of the upper boundary is crucial as the geostrophic velocities and consequently the geostrophic transport increases toward the surface. Hence, in this study, we define the upper boundary of the lower STC branch by using the seasonally varying depth of meridional velocity reversal.
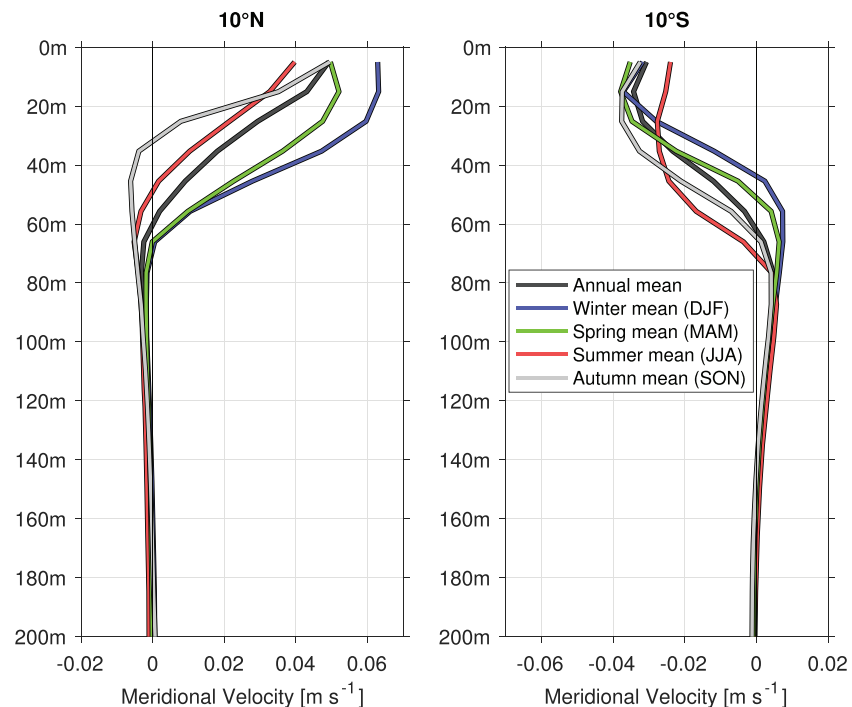

Figure 4. Zonally averaged vertical profiles of meridional velocity for boreal winter (blue), spring (green), summer (red), and autumn (gray) composites as well as for an annual mean (black) along the two sections at 10°N and 10°S from ORA-S4.
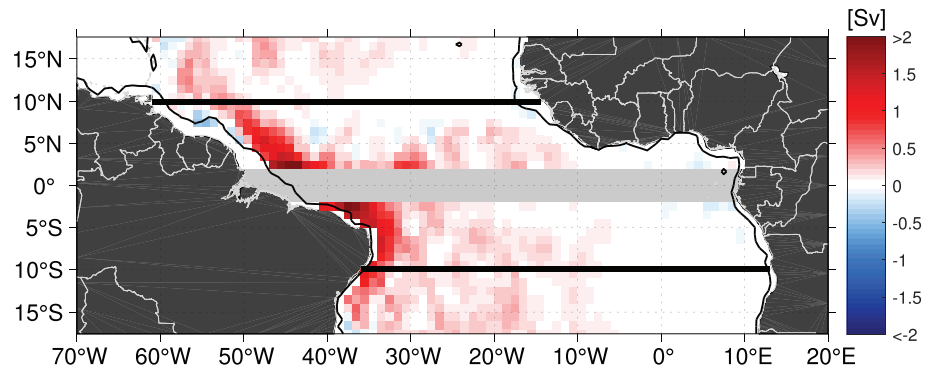
Figure 5. Integrated equatorward geostrophic transport (from the RG-clim) between the seasonally varying interface depth and the 26.0 kg m^{-3} isopycnal for zonal boxes of 1° together with the 1,000-m isobath from the ETOPO1 data set (black contour). The thick black lines indicate the zonal sections at 10°N and 10°S. Note that red colours indicate equatorward transport and blue colours poleward transport.

ORA-S4 provides absolute zonal and meridional velocity data of which the latter are used to determine the depth of meridional velocity reversal d_i (interface depth). The annual mean depth at which poleward velocities change to equatorward velocities at 10°N and 10°S is 60 m. However, the interface depth undergoes a strong seasonal cycle at both latitudes (Figure 4). Consequently, the interface between the horizontal branches of the STCs is defined by a seasonally varying interface depth. The seasonal interface depths for 10°N are 65, 65, 50, and 30 m respectively for winter, spring, summer, and autumn; the corresponding depths for 10°S are 45, 50, 70, and 65 m (Figure 4). In the zonal mean, the equatorward transports are accomplished in the density layer between the seasonally varying interface depth and the 26.0 kg m^{-3} isopycnal in both hemispheres.

The zonal mean is instructive to define the boundaries of the thermocline layer. With this definition, the horizontal distribution of the different meridional pathways of thermocline layer transport can be estimated (Figure 5). Note that at the equator, geostrophic balance does not hold due to the vanishing Coriolis force.
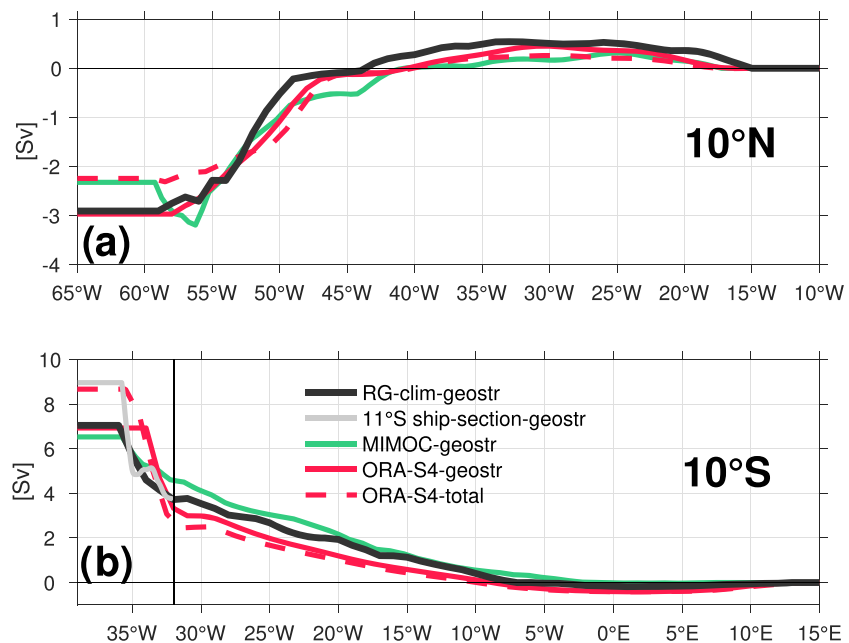

Figure 6. Cumulative meridional transport along (a) 10°N and (b) 10°S integrated from east to west and between the seasonally varying interface depth and the 26.0 kg m^{-3} isopycnal. The black line at 32°W in (b) indicates the most eastern extent of the repeated ship section at 11.5°S at which the western boundary transport from the ship section is added to the accumulated transport of RG-clim at 32°W.

Table 1
Equatorward Transport Between the Seasonally Varying Interface Depth and the 26.0 kg m^{-3} Isopycnal for Different Products at the Two Zonal Sections at 10°N/°S

	10°N				10°S				
	RG-clim	MIMOC	ORA-geostr	ORA-total	RG-clim	MIMOC	ORA-geostr	ORA-total	Ship section
INTϵ	0.2±0.5	0.9±0.3	0.7±0.7	1.2±0.7	3.8±0.8	4.6±0.2	3.0±0.6	2.5±0.5	—
WBϵ	2.7±1.2	1.4±0.5	2.3±0.7	1.0±0.8	3.3±0.6	2.0±0.2	3.9±0.5	6.2±0.7	5.2±0.8
TOTALϵ	2.9±1.3	2.3±0.5	3.0±1.0	2.2±1.1	7.1±1.0	6.5±0.3	6.9±0.7	8.7±0.9	9.0±1.1

Note. At 10°N (10°S), the 50°W (32°W) longitude divides the sections into an interior part (INT) and a western boundary part (WB). Shown is also the zonally accumulated transport (TOTAL) over the whole basin as well as the particular error estimates (see section 3.1 for details).

Hence, the calculations were only carried out poleward of ±2.5°. In both hemispheres, the highest transport values occur at the western boundary with values of more than 2 Sv per 1° close to the equator. The intensified transports at the western boundary are a consistent feature starting at around 15° off the equator in both hemispheres and increasing toward lower latitudes. Transports associated with the southern STC are slightly higher compared to northern hemisphere values. Larger differences in thermocline layer transport are revealed in the interior part of the basin. At 10°S, substantial equatorward transport is observed in the interior basin. Although transport values do not reach the magnitude of the western boundary transports, the interior exchange window at 10°S exists between 30°W to 10°W. In contrast, at 10°N, interior transports east of the western boundary are almost absent in our analysis. However, closer to the equator, meridional transports are observed, though these are more likely to be associated with the TCs due to the missing connection to the subtropics.

At 10°N, weak poleward transport is present east of about 30°W (Figure 6). West of 30°W weak equatorward transport in the interior basin steadily reduces the accumulated poleward transport leading to a net equatorward transport between 0.2 and 1.2 Sv at 50°W (Table 1). Interior transport at 10°N is not obvious in Figure 5 consistent with close to zero accumulated transport east of about 45°W. From 50°W toward the western boundary, additional transport estimates vary between 1.0 Sv (ORA-S4-total) and 2.7 Sv (RG-clim) with MIMOC (1.4 Sv) and ORA-S4-geostr (2.3 Sv) in between this range. Transports from MIMOC-geostr are about 1 Sv smaller, presumably due to the northward flowing NBC at the western boundary which is better resolved due to included hydrographic data from CTD profiles close to the coast and boundary current mapping algorithm. In summary, all products agree for the majority of the 10°N section apart from the most western part of the section where the spread in equatorward transport is highest.

Along 10°S, all geostrophic estimates agree well from the African coast to 32°W (the easternmost longitude of the western boundary ship section). Interior transports in the southern hemisphere add up to about 3.8 Sv (RG-clim). At the western boundary, the transport estimates from RG-clim and ORA-S4-geostr further agree on 3.3 to 3.9 Sv additional transport while MIMOC shows slightly less transport with 2.0 Sv. As an independent measure of the western boundary current transport, we use data from the repeated ship section at 11.5°S (Figure 7). Geostrophic velocity data from the 11.5°S mean ship section at the western boundary produce a contribution of 5.2 Sv resulting in a total southern STC thermocline layer transport of 9.0 Sv (Figure 6b) when added to the RG-clim value at 32°W. In summary, we find a thermocline convergence between 8.8 and 10.9 Sv of which about 2.2 to 3.0 Sv come from the northern and 6.5 to 8.7 Sv are provided by the southern STC. The difference between interior and western boundary transport is most prominent in the northern hemisphere in the RG-clim estimates with essentially no interior transport.

4.2. Surface Transports

We have shown that the lower branches of the STCs encompass water masses toward the equator in a layer between the seasonally varying interface depth and the 26.0 kg m^{-3} isopycnal with a contribution from the southern hemisphere three times higher than that from the northern hemisphere and a higher contribution from the western boundaries than from the interior ocean basins. Equatorward transport leads to convergence in the equatorial regions at thermocline level. There, thermocline water is entrained into the EUC and upwells either along its eastward pathway or reaches the eastern boundary upwelling systems. The STCs are eventually closed by poleward transport in the surface layer driven by meridional Ekman transport. In order to estimate the poleward transport of the upper branches of the STCs, several wind products are used (described in section 2.5). Both hemispheres are divided into an eastern part, where the mean zonal wind
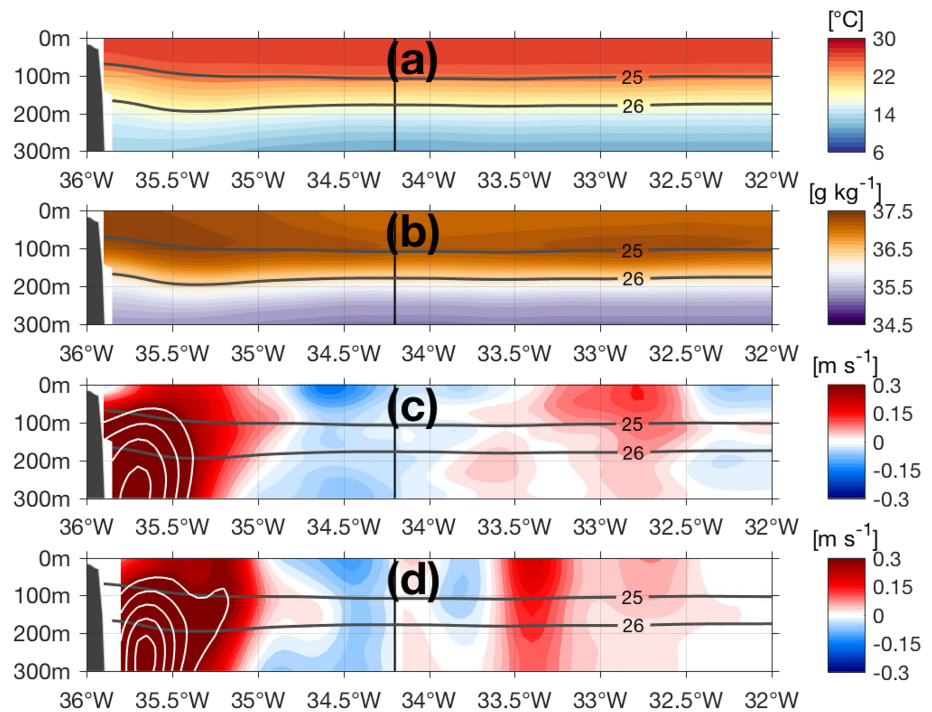
Figure 7. Mean (a) conservative temperature, (b) absolute salinity, (c) meridional/alongshore absolute velocity, and (d) meridional/alongshore geostrophic velocity from the repeated ship section at 11.5°S. Isopycnal surfaces are shown as black contour lines. The black line at 34.2°W marks the longitude at which the ship section turns northwestward (see, e.g., Figure 1). The western boundary of the section is depicted by the topography from the ETOPO1 data set.

stress leads to weak or no equatorward Ekman transports and a western part with poleward Ekman transports generally intensifying toward the western boundary (Figure 8). Meridional Ekman transport maps derived from the other wind products (not shown) agree well on this structure. The accumulated meridional Ekman transport values along the zonal sections at 10°N and 10°S are shown in Table 2. Here, negative transport values indicate southward transport while positive values indicate northward transport. For individual wind products, the Ekman divergence among 10°N and 10°S appears rather symmetric although differences in the strength of the Ekman divergence between the products are found. The symmetry of transport in the surface layer is in contrast to the asymmetric interhemispheric transport distribution at thermocline level. Hence, between 10°N and 10°S, an Ekman divergence of about 20.4 Sv (mean value derived from three wind products) is found and faces a thermocline convergence of about 11.9 Sv (RG-clim including western boundary ship section mean at 10°S).
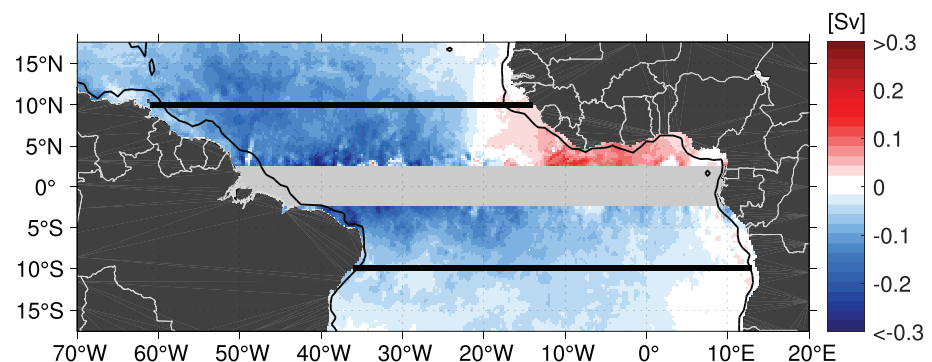

Figure 8. Mean meridional Ekman transport derived from daily ASCAT wind stress between 2007 to 2018. The thick black lines indicate the zonal sections at 10°N and 10°S at which the meridional Ekman transport is accumulated from east to west and the black contour lines show the 1,000-m isobath from the ETOPO1 data set. Note that red colours indicate equatorward transport and blue colours poleward transport.

Table 2
Geostrophic, Ekman, and Net Transport Between the Surface and the Seasonally Varying Interface Depth from Different Products at the Two Zonal Sections at 10°N/°S

	10°N							
	Geostrophic			Ekman			Net	
	RG-clim	MIMOC	ORA-S4	ASCAT	NCEP/NCAR	JRA-55	ORA-S4	ASCAT + RG-clim
INT ϵ	−0.7±0.8	−1.5±0.4	−1.0±0.9	6.1±0.6	5.8±1.9	5.4±0.7	3.4±1.2	5.4
WB ϵ	−1.4±0.9	−1.0±0.4	−0.9±0.6	3.5±0.3	4.4±1.2	3.3±0.4	3.0±0.9	2.1
TOTAL ϵ	−2.1±1.2	−2.5±0.6	−1.9±1.0	9.6±0.7	10.2±2.2	8.7±0.8	6.4±1.4	7.5
	10°S							
	Geostrophic			Ekman			Net	
	RG-clim	MIMOC	ORA-S4	ASCAT	NCEP/NCAR	JRA-55	ORA-S4	ASCAT + RG-clim
INT ϵ	2.6±0.6	4.8±0.2	2.7±0.7	−10.1±0.5	−10.6±1.6	−8.5±0.5	−6.2±0.7	−7.6
WB ϵ	1.2±0.3	0.3±0.1	0.9±0.4	−1.1±0.1	−1.4±0.6	−1.0±0.2	0.7±0.5	0.1
TOTAL ϵ	3.7±0.7	5.1±0.3	3.6±0.8	−11.2±0.5	−12.0±1.7	−9.5±0.5	−5.5±0.8	−7.5

Note. At 10°N (10°S), the 50°W (32°W) longitude divides the sections into an interior part (INT) and a western boundary part (WB). Shown is also the zonally accumulated transport over the whole basin (TOTAL) as well as the particular error estimates (see section 3.1 for details).

However, as we have seen in Figure 2, geostrophic flow is also present in the surface layer and generally counteracts the poleward Ekman transport. Hence, the upper branches of the STCs consist of two opposing meridional transports: poleward Ekman transport and equatorward geostrophic transport. Table 2 also shows the surface layer geostrophic transport from RG-clim, MIMOC, and ORA-S4. We find good agreement among the products as well as a further signature of the interhemispheric asymmetry in equatorward geostrophic transport with about twice as much transport originating in the southern hemisphere (3.6 to 5.1 Sv vs. 1.9 to 2.5 Sv). In contrast to the thermocline layer, geostrophic transport in the surface layer is higher in the interior basin, which is especially the case for the southern hemisphere. In the surface layer, geostrophic transports are opposite to Ekman transports derived from wind products (Table 2). Therefore, the sum of Ekman transport and geostrophic transport can be seen as a net transport. However, the net transport can also be directly estimated from absolute velocities from ORA-S4 (Table 2). Interestingly, interior and western boundary net transport at 10 °N are close to being equal while the southern hemisphere net transport is clearly dominated by interior transport. The same way the subsurface NBUC in the southern hemisphere distributes water to the equator at thermocline level, the surface intensified NBC/Guyana Current in the northern hemisphere withdraws water poleward in the surface layer but to a lesser extent.

The difference in net transports between both methods is relatively small (Table 2) and generally confirms the choice of layer boundaries in this study. It also indicates that the choice of the interface between the upper and the lower branch of the STCs (described in section 3.1) is plausible.

In summary, we observe a surface layer divergence of meridional transport of 14.6 ± 3.4 Sv when considering the sum of an averaged Ekman divergence (20.4 ± 3.1 Sv) and the geostrophic surface convergence from RG-clim (5.8 ± 1.4 Sv). Overall, in combination with the thermocline layer convergence of 11.9 ± 1.7 Sv, a residual of 2.7 ± 3.8 Sv is required to maintain the balance of the STC circulation regime. Sources for the missing transport will be discussed in the next section.

5. Summary and Discussion

This study provides observational estimates for both branches of the Atlantic STCs and compares them to results from a reanalysis product and previous studies. Based on the rapidly increasing data coverage of the world's oceans by Argo floats within the last two decades, Roemmich and Gilson (2009) constructed a hydrographic climatology of which an updated version considering Argo profiles between January 2004 and December 2016 is available. Besides Argo float data, we have made use of another hydrographic climatology, MIMOC (Schmidtko et al., 2013), that additionally includes shipboard CTD data. In this study, the issue of sparse data coverage at the western boundary by Argo floats is further addressed by analyzing data from a repeated ship section at 11.5°S (Hummels et al., 2015) to derive reliable estimates of the western boundary

transport in the STC density range. The analysis is complemented by hydrographic and velocity data from the ORA-S4 reanalysis (Balmaseda et al., 2013).

Previous to the Argo era, the study of Zhang et al. (2003), who estimated STC transports based on hydrographic data, provided a benchmark against which numerical studies compared their results. Our study provides an update of the temporal mean transport estimates of the STCs thereby presenting a 21st century mean state of the Atlantic STCs based on hydrographic and velocity observations. Besides the data sets used here, the most significant changes from this study to the estimates by Zhang et al. (2003) are the definition of the vertical boundaries of the branches of the STCs and the choice of latitude for the southern section. In agreement with Schott et al. (2004) and Rabe et al. (2008), we focused our analysis on zonal sections at 10°N and 10°S while Zhang et al. (2003) chose a southern section along 6°S. Both, 10°N and 10°S, are sufficiently far away from the TCs and the subtropical subduction zones suggesting that transports associated with the STCs must pass these sections. The southern section at 10°S is mainly chosen due to the availability of a repeated ship section along 11.5°S close-by. With the help of spatially high-resolved observational data at the crucial western boundary region, we could show that Argo based observational products as RG-clim likely underestimate the transport at the western boundary at 10°S (e.g., Figure 6 and Table 1). From hydrographic properties along the chosen sections, meridional geostrophic velocity—referenced to the 1,000 dbar meridional displacement derived from YoMaHa'07 (Lebedev et al., 2007)—and isopycnal surfaces are calculated (Figure 2). In general, equatorward geostrophic velocities are observed from the surface down to approximately 26.0 kg m^{-3}. However, in the surface layer, the wind-driven poleward Ekman transport is counteracting the geostrophic flow. Therefore, we suggest to identify the interface depth between the poleward and the equatorward STC branches as the depth at which the meridional velocity reverses and below which the flow is in geostrophic balance. As shown in Figure 4, a seasonally varying interface depth (between 30 to 65 m at 10°N and 45 to 70 m at 10°S) is used for the transport estimation. This definition further takes into account that the isopycnals are sloping upward toward the east (Figure 2). A purely isopycnal definition of the interface leads to an upper boundary that crosses the Ekman layer in the eastern part of the basin and underestimates the thickness of the thermocline layer in the western part. Consequently, it is suggested that the STCs transport water masses toward the equator in a layer between the interface depth and an isopycnal surface. This layer is called thermocline layer or pycnocline layer (e.g., Zhang et al., 2003). The lower boundary of this layer is defined using the zonal mean of meridional transport per 0.2 kg m^{-3} density bin (Figure 4). In both hemispheres, the lower boundary of the thermocline layer is set to 26.0 kg m^{-3}. In previous studies, this thermocline layer has been enclosed by isopycnal layers at the top and bottom. For instance, Zhang et al. (2003) defined their northern hemisphere thermocline layer between 23.2 and 26.0 kg m^{-3} and their southern hemisphere thermocline layer between 23.6 and 26.2 kg m^{-3}, whereas Fratantoni et al. (2000) used two of their six model layers to describe thermocline transports between 25.2 and 26.8 kg m^{-3} and Hazeleger and Drijfhout (2006) used the mixed-layer-depth as the interface between the two STC branches. The vertical resolution in numerical studies is often too coarse to define more precise boundaries.

Following our definition of the thermocline layer boundaries, meridional transports within this layer have been calculated. Unless otherwise noted, the mentioned thermocline layer transports refer to the estimates from the RG-clim. In general, equatorward transports can be divided into transports along the western boundary and within the interior ocean. The boundary is set to 50°W for the northern section and to 32°W for the southern section. We are able to show that for the northern hemisphere STC, the interior exchange window is extremely small (Figure 5) and only exhibits a marginal equatorward transport, not significantly different from zero (Table 1). This is most likely due to the presence of the previously described PV barrier in the northeastern tropical Atlantic (e.g., Harper, 2000; Hazeleger & Drijfhout, 2006) forcing a detour of the equatorward flow. Hence, at 10°N, most of the equatorward transport is accomplished via the western boundary within the recirculation pathway of the NBC (about 2.7 Sv). Closer to the coast, the northward flow of the NBC at the western boundary within the thermocline layer is suggested to reduce the equatorward transport as indicated by MIMOC (see Figure 6a). Johns et al. (1998) found that the NBC at 3°N to 4°N transports about 3 to 5 Sv over the continental shelf of which parts recirculate into the zonal current system in the tropical Atlantic and would not be observed at 10°N. As part of the North Brazil Current Rings Experiment, Garzoli et al. (2003) estimated the annual mean transport due to the rings to be 8 Sv based on 11 rings between November 1998 and June 2000. Clearly, the data coverage at the western boundary in the northern hemisphere introduces an uncertainty to the budget-like transport estimates of the STC branches in this analysis. The thermocline convergence contribution of the northern hemisphere STC is estimated to
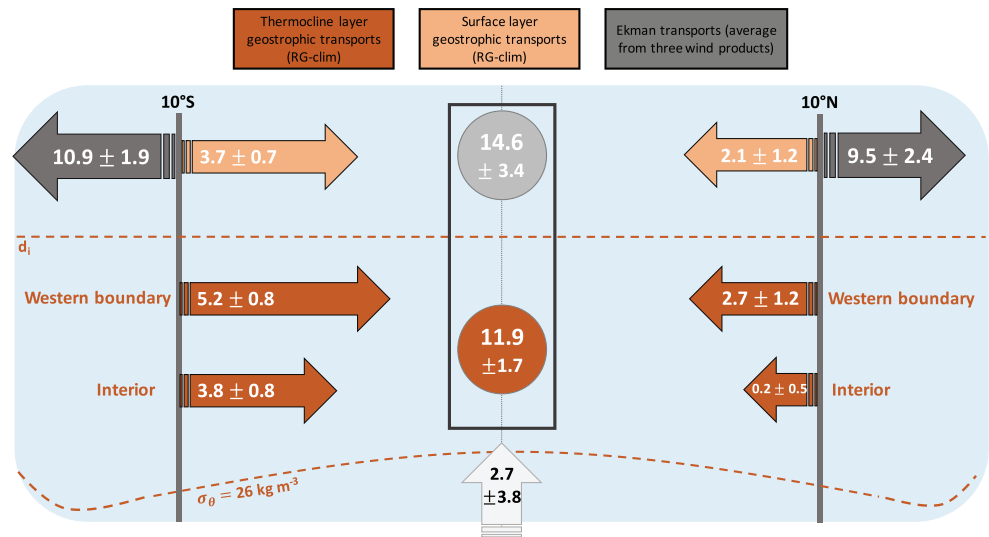
Figure 9. Schematic of particular meridional transport contributions to the Atlantic STCs in [Sv]. Shown are geostrophic transports as estimated by RG-clim (dark orange in the thermocline layer and light orange in the surface layer) in combination with mean ship sections for the western boundary in the southern hemisphere as well as the mean meridional Ekman transport derived from three different wind products (gray). The equatorward transport associated with the lower branch of the STCs occurs between the seasonally varying interface depth d_i and the 26.0 kg m^{-3} isopycnal. At the equator, Ekman divergence within the surface layer forces upwelling and poleward Ekman transport associated with the upper branch of the STCs. An estimated 2.7 Sv (light gray arrow) has to enter the thermocline layer in the tropics to balance the transport estimates. Note that due to the uncertainty at the western boundary at 10°N, this value is likely to be higher.

be approximately 2.9 Sv (2.7 Sv western boundary and 0.2 Sv interior). Due to the superposition of the AMOC on equatorward transport at the western boundary and the absence of a PV barrier in the eastern part of the basin, the southern hemisphere STC is significantly stronger than its northern counterpart (e.g., Fratantoni et al., 2000). We show that at 10°S, an interior transport of about 3.8 Sv is observed in a window from about 10°W to 32°W (Figure 6b). At the western boundary, the horizontal resolution and the representation of the western boundary current among the products introduce an uncertainty and a range of equatorward transport between 2.0 and 6.2 Sv is estimated (Figure 6b and Table 1). When transport from the mean ship section is added to the 32°W value of the RG-clim, an equatorward thermocline transport of 9.0 Sv along 10°S results (Figure 9). Note that the mean section consists of five individual sections of shipboard velocity measurements. Although those sections are distributed relatively even throughout the seasons, an uncertainty remains about the representation of the mean state. However, moored observations reassuringly show a similar mean (Hummels et al., 2015).

In summary, we find a thermocline layer convergence of 11.9 Sv equatorward transport (considering RG-clim estimates in the northern hemisphere and combined RG-clim and ship section estimates in the southern hemisphere) between 10°N and 10°S which is about 3 Sv less than previously estimated by Zhang et al. (2003). This difference can at least partly be explained by the different choices of vertical thermocline layer boundaries as described above. Especially in the eastern part of the basin, choosing the depth of meridional velocity reversal as the upper boundary leads to a smaller layer thickness compared to an isopycnal boundary as used by Zhang et al. (2003).

In the surface layer, wind products are averaged to a mean Ekman divergence of 20.4 Sv (Table 2) which is slightly smaller than in previous studies such as Schott et al. (2004) who report 21 and 23 Sv of zonally integrated annual-mean Ekman divergence for NCEP reanalysis and ERS.1,2 scatterometer data respectively for an earlier time period. The wind-driven Ekman transport is reduced by the geostrophic transport (integrated from the surface to the interface depth) and results in the net meridional transport in the surface layer.

The sum of the STC related equatorward and poleward transport contributions yields a residual of 2.7 Sv which is suggested to be upwelled from below the thermocline as part of the interhemispheric AMOC return flow (Figure 9). This number is smaller than in previous studies in which estimates of the return flow

of the thermohaline circulation ranged between 6 and 10 Sv from below the thermocline layer across the 26.2 kg m^{-3} isopycnal (Roemmich, 1983). Hazeleger and Drijfhout (2006) and Lux et al. (2001) arrived at similar values of 5.5 and 7.5 Sv, respectively. The most likely explanation for this discrepancy is the underestimation of the northward western boundary current north of the equator in our study. Especially estimates at the western boundary in the northern hemisphere are still uncertain and more ship sections and Argo float data are needed to derive more reliable transport values and to decrease the uncertainty.

This study provides an update for observational estimates of Atlantic STC transports and aims to represent the 21st century mean STCs from an observational perspective. Observations from the Argo program are suitable to represent the geostrophic branches of the Atlantic STCs. This improvement in data coverage is especially important when considering interannual to decadal variability of STC transports which so far could not be captured by observations. Building on the definitions for the STC branches and their boundaries developed here, future work will focus on the impact of seasonal to interannual variability of both transport and water mass properties on SST variability to gain more insight on the responsible mechanism (Gu & Philander, 1997; Kleeman et al., 1999).

References

Amante, C., & Eakins, B. W. (2009). ETOPO1 1 arc-minute global relief model: Procedures, data sources and analysis, NOAA Technical Memorandum NESDIS NGDC-24 (October) 19pp. https://doi.org/10.7289/V5C8276M

Balmaseda, M. A., Mogensen, K., & Weaver, A. T. (2013). Evaluation of the ECMWF ocean reanalysis system ORAS4. *Quarterly Journal of the Royal Meteorological Society*, *139*, 1132–1161. https://doi.org/10.1002/qj.2063

Farneti, R., Dwivedi, S., Kucharski, F., Molteni, F., & Griffies, S. M. (2014). On Pacific subtropical cell variability over the second half of the twentieth century. *Journal of Climate*, *27*(18), 7102–7112. https://doi.org/10.1175/JCLI-D-13-00707.1

Fratantoni, D. M., Johns, W. E., Townsend, T. L., & Hurlburt, H. E. (2000). Low-latitude circulation and mass transport pathways in a model of the tropical Atlantic Ocean* *Journal of Physical Oceanography*, *30*(8), 1944–1966. https://doi.org/10.1175/1520-0485(2000)030<1944:LLCAMT>2.0.CO;2

Garzoli, S. L., Ffield, A., & Yao, Q. (2003). North Brazil Current rings and the variability in the latitude of retroflection. *Interhemispheric Water Exchange in the Atlantic Ocean*, *68*, 357–374. https://doi.org/10.1016/S0422-9894(03)80154-X

Gu, D., & Philander, S. G. H. (1997). Interdecadal climate fluctuations that depend on exchanges between the tropics and extratropics. *Science*, *275*(5301), 805–807. https://doi.org/10.1126/science.275.5301.805

Harper, S. (2000). Thermocline ventilation and pathways of tropical-subtropical water mass exchange. *Tellus, Series A: Dynamic Meteorology and Oceanography*, *52*(3), 330–345. https://doi.org/10.3402/tellusa.v52i3.12269

Hazeleger, W., de Vries, P., & Friocourt, Y. (2003). Sources of the Equatorial Undercurrent in the Atlantic in a high-resolution ocean model. *Journal of Physical Oceanography*, *33*(4), 677–693. https://doi.org/10.1175/1520-0485(2003)33<677:SOTEUI>2.0.CO;2

Hazeleger, W., & Drijfhout, S. (2006). Subtropical cells and meridional overturning circulation pathways in the tropical Atlantic. *Journal of Geophysical Research*, *111*, C03013. https://doi.org/10.1029/2005JC002942

Hummels, R., Brandt, P., Dengler, M., Fischer, J., Araujo, M., Veleda, D., & Durgadoo, J. V. (2015). Interannual to decadal changes in the western boundary circulation in the Atlantic at 11°S. *Geophysical Research Letters*, *42*, 7615–7622. https://doi.org/10.1002/2015GL065254

Inui, T., Lazar, A., Malanotte-Rizzoli, P., & Busalacchi, A. J. (2002). Wind stress effects on subsurface pathways from the subtropical to tropical Atlantic. *Journal of Physical Oceanography*, *32*(8), 2257–2276. https://doi.org/10.1175/1520-0485(2002)032<2257:WSEOSP>2.0.CO;2

Johns, W. E., Lee, T. N., Beardsley, R. C., Candela, J., Limeburner, R., & Castro, B. (1998). Annual cycle and variability of the North Brazil Current. *Journal of Physical Oceanography*, *28*(1), 103–128. https://doi.org/10.1175/1520-0485(1998)028<0103:ACAVOT>2.0.CO;2

Kleeman, R., McCreary, J. P., & Klinger, B. A. (1999). A mechanism for generating ENSO decadal variability. *Geophysical Research Letters*, *26*(12), 1743. https://doi.org/10.1029/1999GL900352

Kopte, R., Brandt, P., Claus, M., Greatbatch, R. J., & Dengler, M. (2018). Role of Equatorial Basin-mode resonance for the seasonal variability of the Angola current at 11°S. *Journal of Physical Oceanography*, *48*(2), 261–281. https://doi.org/10.1175/JPO-D-17-0111.1

Kuntz, L. B., & Schrag, D. P. (2018). Hemispheric asymmetry in the ventilated thermocline of the tropical pacific. *Journal of Climate*, *31*(3), 1281–1288. https://doi.org/10.1175/JCLI-D-17-0686.1

Lazar, A., Inui, T., Malanotte-Rizzoli, P., Busalacchi, A. J., Wang, L., & Murtugudde, R. (2002). Seasonality of the ventilation of the tropical Atlantic thermocline in an ocean general circulation model. *Journal of Geophysical Research*, *107*(C8), 3104. https://doi.org/10.1029/2000JC000667

Lebedev, K. V., Yoshinari, H., Maximenko, N. A., & Hacker, P. W. (2007). YoMaHa'07: Velocity data assessed from trajectories of Argo floats at parking level and at the sea surface. *IPRC Technical Note*, *2*(4), 20.

Liu, Z., Philander, S. G. H., & Pacanowski, R. C. (1994). A GCM study of tropical-subtropical upper-ocean water exchange. *Journal of Physical Oceanography*, *24*(12), 2606–2623. https://doi.org/10.1175/1520-0485(1994)024<2606:AGSOTU>2.0.CO;2

Lu, P., McCreary, J. P., & Klinger, B. A. (1998). Meridional circulation cells and the source waters of the Pacific Equatorial Undercurrent. *Journal of Physical Oceanography*, *28*(1), 62–84. https://doi.org/10.1175/1520-0485(1998)028<0062:mccats>2.0.co;2

Lübbecke, J. F., Böning, C. W., & Biastoch, A. (2008). Variability in the subtropical-tropical cells and its effect on near-surface temperature of the equatorial Pacific: A model study. *Ocean Science*, *4*(1), 73–88. https://doi.org/10.5194/os-4-73-2008

Lux, M., Mercier, H., & Arhan, M. (2001). Interhemispheric exchanges of mass and heat in the Atlantic Ocean in January-March 1993. *Deep-Sea Research Part I: Oceanographic Research Papers*, *48*(3), 605–638. https://doi.org/10.1016/S0967-0637(00)00033-9

Malanotte-Rizzoli, P., Hedstrom, K., Arango, H., & Haidvogel, D. B. (2000). Water mass pathways between the subtropical and tropical ocean in a climatological simulation of the North Atlantic ocean circulation. *Dynamics of Atmospheres and Oceans*, *32*(3-4), 331–371. https://doi.org/10.1016/S0377-0265(00)00051-8

McCreary, J. P., & Lu, P. (1994). Interaction between the subtropical and equatorial ocean circulations: The subtropical cell. *Journal of Physical Oceanography*, *24*(2), 466–497. https://doi.org/10.1175/1520-0485(1994)024<0466:IBTSAE>2.0.CO;2

McDougall, T. (2017). Getting started with TEOS-10 and the Gibbs Seawater (GSW) Oceanographic Toolbox.

McPhaden, M. J., & Zhang, D. (2002). Slowdown of the meridional overturning circulation in the upper Pacific Ocean. *Nature*, *415*, 603–608. https://doi.org/10.1038/415603a

McPhaden, M. J., & Zhang, D. (2004). Pacific Ocean circulation rebounds. *Geophysical Research Letters*, *31*, L18301. https://doi.org/10.1029/2004GL020727

Oschlies, A., Brandt, P., Stramma, L., & Schmidtko, S. (2018). Drivers and mechanisms of ocean deoxygenation. *Nature Geoscience*, *11*(7), 467–473. https://doi.org/10.1038/s41561-018-0152-2

Peña-Izquierdo, J., van Sebille, E., Pelegrí, J. L., Sprintall, J., Mason, E., Llanillo, P. J., & Machín, F. (2015). Water mass pathways to the North Atlantic oxygen minimum zone. *Journal of Geophysical Research: Oceans*, *120*, 3350–3372. https://doi.org/10.1002/2014JC010557

Rabe, B., Schott, F. A., & Köhl, A. (2008). Mean circulation and variability of the tropical Atlantic during 1952–2001 in the GECCO assimilation fields. *Journal of Physical Oceanography*, *38*(1), 177–192. https://doi.org/10.1175/2007JPO3541.1

Roemmich, D. (1983). The balance of geostrophic and Ekman transports in the tropical Atlantic Ocean. *Journal of Physical Oceanography*, *13*(8), 1534–1539.

Roemmich, D., & Gilson, J. (2009). The 2004-2008 mean and annual cycle of temperature, salinity, and steric height in the global ocean from the Argo Program. *Progress in Oceanography*, *82*(2), 81–100. https://doi.org/10.1016/j.pocean.2009.03.004

Schmidtko, S., Johnson, G. C., & Lyman, J. M. (2013). MIMOC: A global monthly isopycnal upper-ocean climatology with mixed layers. *Journal of Geophysical Research: Oceans*, *118*, 1658–1672. https://doi.org/10.1002/jgrc.20122

Schott, F. A., Dengler, M., Zantopp, R. J., Stramma, L., Fischer, J., & Brandt, P. (2005). The shallow and deep western boundary circulation of the South Atlantic at 5° 11°S. *Journal of Physical Oceanography*, *35*, 2031–2053. https://doi.org/10.1175/JPO2813.1

Schott, F. A., Fischer, J., & Stramma, L. (1998). Transports and pathways of the upper-layer circulation in the western tropical Atlantic. *Journal of Physical Oceanography*, *28*(10), 1904–1928. https://doi.org/10.1175/1520-0485(1998)028<1904:TAPOTU>2.0.CO;2

Schott, F. A., McCreary, J. P., & Johnson, G. C. (2004). Shallow overturning circulations of the tropical-subtropical oceans. *Earth Climate: The Ocean-Atmosphere Interaction. Geophysical Monography Series*, *147*, 261–304. https://doi.org/10.1029/147GM15

Stramma, L., & Schott, F. A. (1999). The mean flow field of the tropical Atlantic Ocean. *Deep-Sea Research Part II: Topical Studies in Oceanography*, *46*(1-2), 279–303. https://doi.org/10.1016/S0967-0645(98)00109-X

Tsuchiya, M. (1986). Thermostads and circulation in the upper layer of the Atlantic Ocean. *Progress in Oceanography*, *16*, 235–267.

Zhang, D., McPhaden, M. J., & Johns, W. E. (2003). Observational evidence for flow between the subtropical and tropical Atlantic: The Atlantic subtropical cells. *Journal of Physical Oceanography*, *33*, 1783–1797. https://doi.org/10.1175/2408.1